Investigation of a surface mounted pm machine concept with 3d-flux paths, modular stator and amorphous material

Gonzalez, Adolfo Garcia; Wang, Dong; Rasmussen, Peter Omand

Published in:
Proceedings of 2019 IEEE International Electric Machines & Drives Conference (IEMDC)

DOI (link to publication from Publisher):
10.1109/IEMDC.2019.8785277

Publication date:
2019

Document Version
Accepted author manuscript, peer reviewed version

Investigation of a Surface Mounted PM Machine Concept with 3D-Flux Paths, Modular Stator and Amorphous Material

Adolfo Garcia Gonzalez
Energy Technology Department
Aalborg University
Aalborg, Denmark
agg@et.aau.dk

Dong Wang
Energy Technology Department
Aalborg University
Aalborg, Denmark
dwa@et.aau.dk

Peter Omand Rasmussen
Energy Technology Department
Aalborg University
Aalborg, Denmark
por@et.aau.dk

***Abstract*—This paper deals with the design and investigation of a surface mounted machine concept targeted at the efficient recycling of rare-earth materials used in permanent magnets. The proposed machine has an outer rotor, single phase and a modular stator. In addition, the use of laminated iron based amorphous material is investigated. The implementation of this type of material in electrical machines is of interest due to their performance in terms of reduced losses when compared with standard electrical steel. However, the widespread use of amorphous materials is limited mainly due to their hardness and brittleness that make their processing (i.e. cutting and punching) a challenging task. Hence, an alternative for the use of such material is proposed in this paper, with the combination of both laminated C-shaped amorphous cores and a modular stator. 3D-FEM calculations of various parameters such as back-EMF, torque, inductance and losses, were validated with measurements performed on a demonstrator.**

***Index Terms*—amorphous materials, magnet losses, 3D-FEM, 3D-flux, modular stator, recyclability**

I. Introduction

The criticality of Rare Earth Elements (REEs) has increased awareness of the recycling of Permanent Magnet (PM) material in electrical machines [1]. Although there are methods available for recycling REEs, some of them are either high energy consuming or have a large environmental impact or may not be used at a large scale [2]. Therefore, developing new machine topologies with special focus on recycling of PM material have obtained special interest. The machine proposed in this work is an attempt to evaluate an alternative topology with non-traditional materials. The use of amorphous materials in electrical machines, have been studied on various types of machines [3] [4] [5] [6]. Furthermore, the use of laminated C-shaped amorphous cores has been investigated with both FEM simulations performed on a linear machine [7] and the experimental investigation of a claw pole transverse flux machine [4]. Regarding designs focused on recyclability of electrical machines, few work has been found [8]. Hence, the main goal of this paper is to propose an electrical machine design, aiming to the recyclability of the PMs, concurrently implementing amorphous material. In Section II both the definition of the concept and the description of the working principle are carried out. In Section III the assembly and the model built in 3D-FEM are explained. In Section IV the results of both calculations and measurements are presented and discussed. In Section V conclusions are drawn and future work is proposed.

II. Description of the Proposed Machine

A. Definition of the Concept

Ideally, having a machine with a large number of poles is of interest since it allows to improve the torque capability. However, an increased number of poles results in the increment of the iron losses in the stator, since these are proportional to the square of the frequency. Although the use of amorphous materials might be beneficial due to their intrinsic low value of specific losses, their magnetic properties might be degraded during their handling, cutting and punching. Hence, the use of laminated C-shaped amorphous cores [9] [10] is proposed as an alternative in order to restrict such degradation. As mentioned above, the use of this type of cores have been studied previously with both FEM simulations [7] and experimental results [4]. However, the machine proposed in this paper is based on the axial flux machine in Fig. 1 [11] [12] [13]. After few modifications applied to the stator core and the rotor in Fig. 2a, the geometry shown in Fig. 2b is obtained. That is, the axial air-gap has been modified in such fashion, that the result is a radial air-gap. Additionally, the stator core has been transformed to a C-shaped magnetic path, allowing the use of C-shaped cores and consequently, the use of laminated amorphous materials, as illustrated in Fig. 3. In order to simplify the manufacturing process, the remaining pieces (i.e. shaft, rotor back and end plates) of a HUB type, radial flux machine were re-used and a stator frame was built in order to house two laminated C-shaped cores of amorphous material. Fig. 4 shows the parts used for assembling the demonstrator.

B. Description of the Working Principle

The working principle is described in Fig. 5. When the permanent magnets on the rotor are aligned with the stator

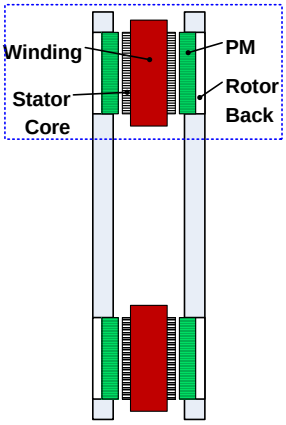

Fig. 1: Double sided internal salient pole stator and external twin rotor AFM.

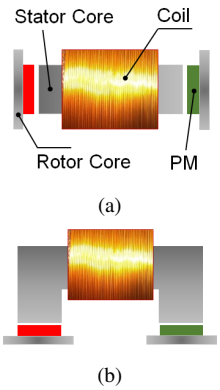

Fig. 2: Definition of the geometry of the machine proposed.

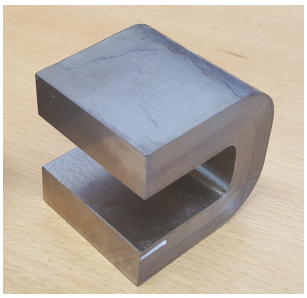

Fig. 3: C-shaped iron based laminated amorphous material 2605SA1 [9].

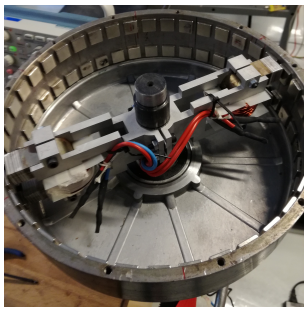

Fig. 4: Assembly of the demonstrator.

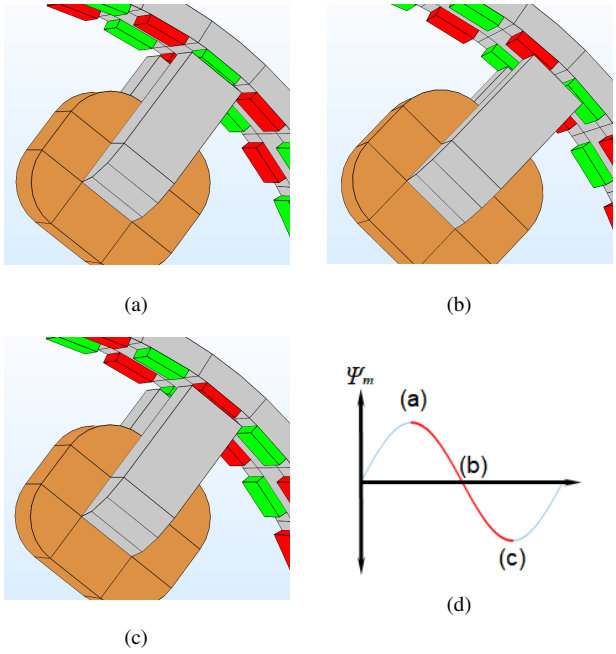

Fig. 5: Working principle.

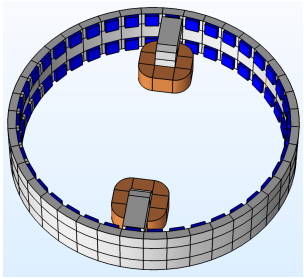

Fig. 6: 3D-FEM model geometry.

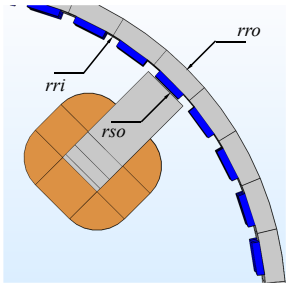

Fig. 7: Main dimensions of the demonstrator, *xy*-plane.

module as in Fig. 5a, the PM flux Ψ_m is maximum. If it is assumed that the rotor is travelling to the right for half a period, the position illustrated in Fig. 5b is reached. Hence, Ψ_m is equal to zero. Finally, when the rotor travels an additional half a period as in Fig. 5c, the PMs in the rotor are aligned with the stator modules but with opposite polarity. Therefore, a minimum is reached. The variation of Ψ_m with the displacement of the rotor is of sinusoidal nature as it is shown in Fig. 5d. Thus, the proposed machine may be driven simply as other PM machines with sinusoidal flux linkage/back-EMF.

III. Assembly and FEM Modelling

A. Main Dimensions

Once the dimensions of the active part of the machine were fixed, the construction of a 3D-FEM model was carried out. The main dimensions of the demonstrator are summarized in Table I. New magnets and iron based amorphous cores were obtained for building the new active part of the demonstrator. In addition, it was necessary to build a supporting frame for the stator modules and the windings. Fig. 6 shows the 3D-FEM modelled geometry where each one of the modules is included along with the PMs, in dark blue, mounted on the rotor cylinder. Additionally, Fig. 7 shows the definition of the main dimensions of the demonstrator. A detailed picture of the stator structure (i.e. coil, stator C-shaped core and supporting frame) is shown in Fig. 8. The test set-up is described in Fig. 9, and the machine was driven as a generator.

IV. Analysis of Results

A. Back-EMF

Fig. 10 shows the waveform of back-EMF measured and calculated at 100 rpm. Although the calculated back-EMF has a similar waveform when compared with measurements,

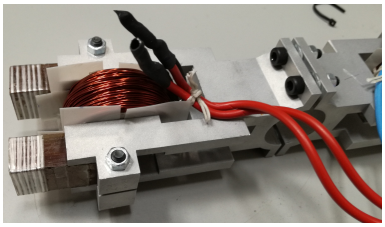

Fig. 8: Assembly of the coil and stator module to the supporting frame.

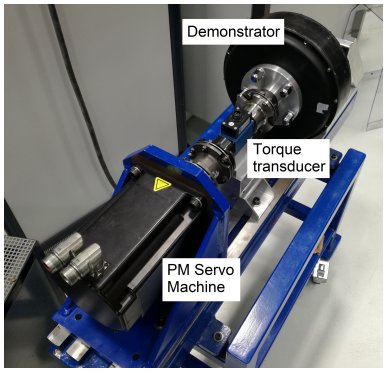

Fig. 9: Test bench used for experiment.

a deviation of approximately 11.8% was obtained. There are several factors that introduce uncertainties in the calculation of this parameter.

- The PMs were modelled in 3D-FEM with the curvature of the inner radius of the rotor rri. However, these are of rectangular shape.
- There might be deviations in the length of the air-gap during the assembly process.

Additional measurements of back-EMF at speeds of 200, 300, 400 and 500 rpm are reported in Fig. 11. The deviation between measured and calculated values remained at a value of approximately 12%.

TABLE I: Main dimensions of the demonstrator.

Dimension	**Value**
Rotor outer radius rro [mm]	139
Rotor inner radius rri [mm]	128
Stator outer radius rso [mm]	127.5
Stack Length [mm]	52
Air-gap length [mm]	0.5
PM thickness [mm]	3
PM width [mm]	15
PM length [mm]	15
PM remanence B_r [T]	1.37
Number of turns per coil	150
Pole pairs	20

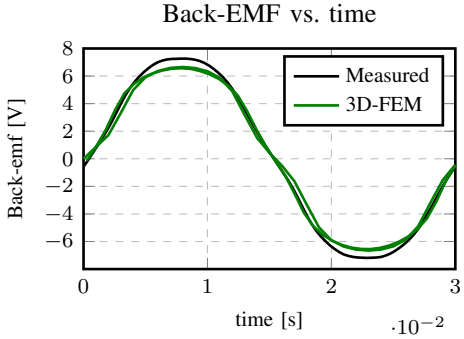

Fig. 10: Back-EMF measured and calculated at 100 rpm.

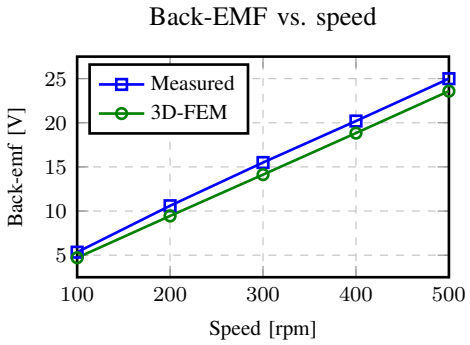

Fig. 11: Back-EMF measured and calculated at various speeds.

TABLE II: Inductance measured and calculated.

Inductance [mH]	
Measured	11.3
3D-FEM	10.3

B. Estimation of the Inductance

For calculating the inductance, the PMs on the rotor were modelled as air and a current applied to the windings. Then the inductance L_a was estimated as:

$$L_a = \frac{\lambda_a}{I_a} \tag{1}$$

Where λ_a is the flux linkage due to the applied current I_a. In contrast, the measurement of the inductance was performed with a Precision Magnetics Analyzer© equipment. The calculations yielded a deviation of 8.9%.The results are summarized in Table II.

C. Estimation of No-Load Losses

The no-load losses p_0 (i.e. bearings, stator iron, PM and rotor back losses) were measured with two different approaches:

- *Case 1:* The machine running at no-load. The product of torque and mechanical speed of the rotor corresponds to the total no-load losses of the machine. That is, $p_0 = T_0 \cdot \omega_{mech}$.
- *Case 2:* A spin down test was performed. The rotor was pulled to rotate and decaying waveform of back-EMF was recorded. The no-load losses were estimated by quadratic fitting of the expression $p_0 = J_m \cdot d\omega_{mech}/dt \cdot \omega_{mech}$. Where J_m is the moment of inertia of the machine.

The results are shown in Fig. 12 showing a good agreement. With *Case 1* as reference, the deviation of *Case 2* was estimated in a range of 9.7 to 19%. Such deviation might be result of the numerical approach that is required for its calculation, and the dependence on the accurate estimation of the inertia.

D. Segregation of the Losses

1) PM and Rotor Back Losses: Generally, PM losses due to slotting effect are insignificant. However, the study of these losses become relevant as a result of the changes of permeance

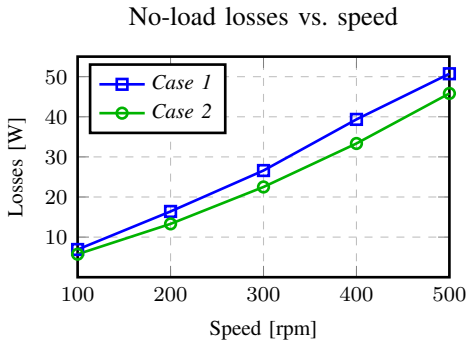

Fig. 12: No-load losses vs. speed.

TABLE III: Parameters used for calculation of losses.

Resistivity	**Value** [$\mu\Omega$/m]
Rotor back ρ_{fe}	0.1
PM ρ_{PM}	0.8

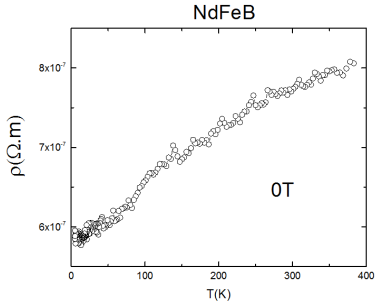

Fig. 13: PM resistivity vs. temperature [17].

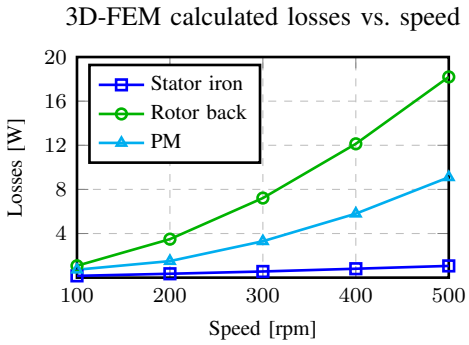

Fig. 14: 3D-FEM calculated losses vs. speed.

seen by the PMs due to the modular structure of the stator (i.e. large air openings between stator modules). In [14] and [15] analytical approximations are proposed. However, neither 2D-FEM nor analytical approaches yield reliable results since such models are appropriate when the length of the PMs is much larger than the thickness [16]. In order to validate the calculated values with the measurements, PM and rotor back losses were estimated with 3D-FEM simulations. The conductivity of the PMs was acquired from measurements performed to samples of sintered magnets of similar quality by the Physical Property Measurement System PPMS of Quantum Design® [17]. The variation of the resistivity with temperature is shown in Fig. 13. The conductivity of iron was assigned to the rotor back region. The values of conductivity implemented in the calculations are summarized in Table III.

2) Stator Iron Losses: The calculation of the iron losses in the stator modules was performed in order to validate the hypothesis of low iron losses in laminated amorphous materials exposed in Section I. The method proposed in [18] was followed. Therefore, a Fourier transformation of the waveform of the magnetic flux density at each finite element in the stator core region was applied to the radial, tangential and axial components of the magnetic flux density, $\hat{b}_r$, $\hat{b}_t$ and $\hat{b}_z$. The results are shown in Fig. 14 along with the calculated values of PM and rotor back losses.

As it was expected, the losses in the stator are significantly low, showing a linear behaviour and reaching a maximum value of approximately 1 W at 500 rpm. Thus, showing the convenience of the use of this type of material. Regarding the PM and rotor back losses, their increment is proportional to the square of the speed, confirming the significant slotting effect, due to the modular structure of the stator.

3) Bearing Losses: In order to perform the measurement of the bearing losses, it was necessary to extract the stator assembly (Fig. 8) (i.e. supporting frames, coils and stator modules) out of the demonstrator. Then, the machine was run and measurements of torque and speed were registered. The bearing losses were estimated as the product of the measured torque and the rotational speed, that is, $p_{bear} = T_0' \cdot \omega_{mech}$. The measured bearing losses are illustrated in Fig. 15. Once the bearing losses were measured, it was possible to contrast both measured and calculated values of no-load losses p_0. The results are shown in Fig. 16, where the calculated values of no-load losses are the summation of the calculated PM, stator iron, rotor back losses and the measured bearing losses. On the other hand, the measured values of p_0 illustrated in Fig. 16 correspond to the values of *Case 1* calculated in Section IV-C.

A maximum deviation of approximately 10.7% was obtained at 500 rpm. The source of such deviation might be the uncertainties in the measurements (e.g. vibration, misalignment of the test set-up, etc.), which might result in the underestimation of the measured losses. Additionally, the uncertainty of the conductivity of the back iron, which material is unknown and as described in Section IV-A the air-gap uncertainties. The distribution of the current density in the PMs due to slotting effect is shown in Fig. 17.

E. Estimation of Torque

A resistive load R_{load} was connected to the terminals of the machine and measurements of torque, current, voltage and power factor were registered at 100, 200, 300, 400 and 500 rpm. In all cases, the resistive load was kept fixed. Fig. 18 shows the equivalent circuit of the test. The power factor at the load is approximately unity given the predominantly resistive nature of the load. Therefore, the current I_s and voltage V_s

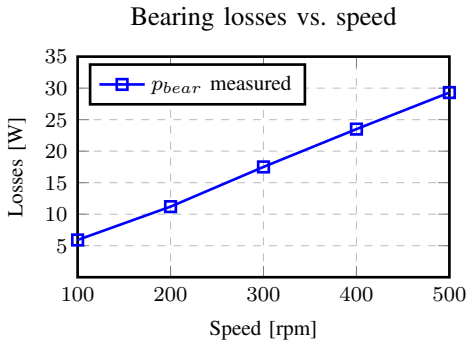

Fig. 15: Bearing losses vs. speed.

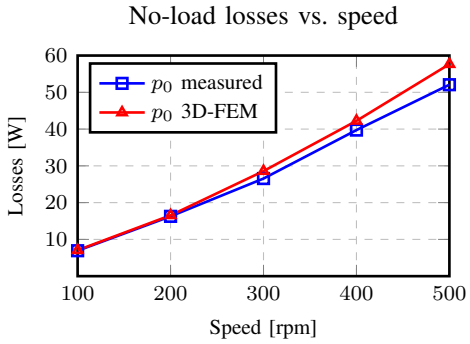

Fig. 16: No-load losses vs. speed.

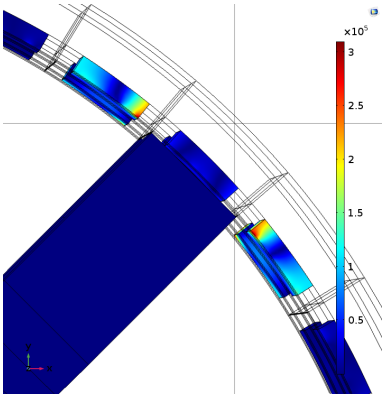

Fig. 17: PM current density at 100 rpm, t=4.6 ms.

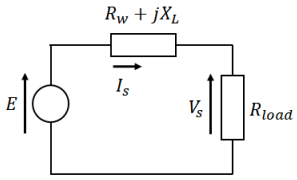

Fig. 18: Equivalent circuit of load test.

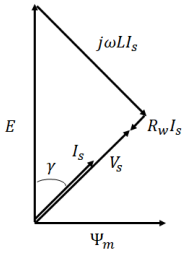

Fig. 19: Phasor diagram in generator mode.

are in phase, as shown in the phasor diagram in Fig. 19. In order to calculate the air-gap torque T_{em} both the amplitude and angle of I_s were required. The current as phasor may be estimated as:

$$\overline{I_s} = \frac{\overline{E}}{R_w + R_{load} + j\omega L} \tag{2}$$

Where $\overline{E}$ is the measured back-EMF, R_w and L are the measured winding resistance and inductance, respectively. Such currents were applied to the FEM models and the torque was calculated. Since the machine was operating as a generator, the measured shaft torque T_{shaft}, the air-gap torque T_{em} and the no-load losses p_0 follow the relation:

$$T_{shaft} = T_{em} + \frac{p_0}{\omega_{mech}} \tag{3}$$

The results are shown in Fig. 20. As it is observed, from measurements, the torque does not increase with the increment of the current I_s. Furthermore, its value starts reducing due to the variation of the load angle γ. The calculated torque follows a similar trend as the measured values. However, the large deviations (approx. 21.6%) might be caused by uncertainties in the measurements for the reasons exposed in Section IV-D3.

V. Conclusions and Future Work

A single phase PM surface mounted machine topology is proposed in which the use of amorphous material is investigated. The modular structure of the stator showed to be easily assembled and disassembled, which might be convenient when addressing the recyclability of the PMs. However, further evaluation of the recyclability potential is required. Additionally, various parameters such as back-EMF, inductance and losses were validated with measurements. Due to the modularity of the motor, it was possible to perform a segregation of the no-load losses in order to evaluate the rotor losses due to slotting effect. Furthermore, as PM losses are increasing with the square of the speed, a surface mounted rotor structure might not be convenient for a machine either running at higher speeds or with a higher pole count. Alternatives such as PM segmentation, and the use of bonded PMs are proposed as future work in the limitation of PM losses.

In addition to the rotor topology studied in this paper, the

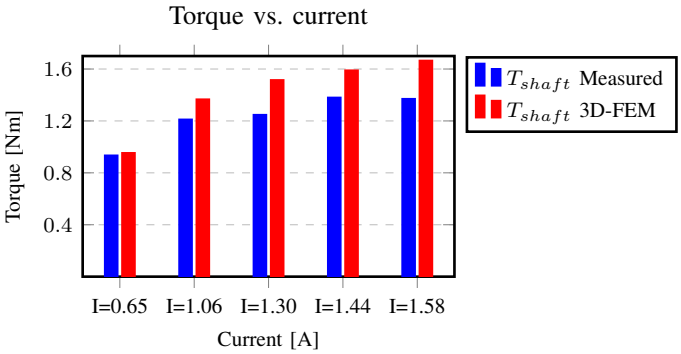

Fig. 20: Torque vs. current comparison.

geometry presented in Fig. 2b allows further modifications. Consequently, it would be possible to consider various rotor topologies (e.g. interior permanent magnet). Hence, the permanent magnets would be protected from the variation of the permeance of the air-gap, which might be beneficial in the reduction of the PM losses.

Unfortunately, the re-use of the parts of a larger motor introduced a large value of bearing losses, which results in a low value of efficiency for this demonstrator (approximately 30%). However, this might be improved by the construction of a complete 3-phase machine, adding stator modules to the structure, consequently improving the torque production. Finally, the concept was demonstrated to work and showed a fair agreement with the calculated values.

ACKNOWLEDGMENT

The research leading to the results presented in this article has been funded by the European Community's Horizon 2020 Programme ([H2010/2014-2019]) under Grant Agreement no. 674973 (MSCA-ETN DEMETER). This publication reflects only the authors view, exempting the Community from any liability. Project website http://etn-demeter.eu/.

REFERENCES

[1] T. Elwert, D. Goldmann, F. Roemer, and S. Schwarz, "Recycling of ndfeb magnets from electric drive motors of (hybrid) electric vehicles," *Journal of Sustainable Metallurgy*, vol. 3, no. 1, pp. 108–121, Mar 2017. [Online]. Available: https://doi.org/10.1007/s40831-016-0085-1

[2] Y. Yang, A. Walton, R. Sheridan, K. Güth, R. Gauß, O. Gutfleisch, M. Buchert, B.-M. Steenari, T. Van Gerven, P. T. Jones, and K. Binnemans, "Ree recovery from end-of-life ndfeb permanent magnet scrap: A critical review," *Journal of Sustainable Metallurgy*, vol. 3, no. 1, pp. 122–149, Mar 2017. [Online]. Available: https://doi.org/10.1007/s40831-016-0090-4

[3] Y. Enomoto, M. Ito, H. Koharagi, R. Masaki, S. Ohiwa, C. Ishihara, and M. Mita, "Evaluation of experimental permanent-magnet brushless motor utilizing new magnetic material for stator core teeth," *IEEE Transactions on Magnetics*, vol. 41, no. 11, pp. 4304–4308, Nov 2005.

[4] N. Dehlinger and M. R. Dubois, "Clawpole transverse flux machines with amorphous stator cores," in *2008 18th International Conference on Electrical Machines*, Sep. 2008, pp. 1–6.

[5] Z. Wang, Y. Enomoto, M. Ito, R. Masaki, S. Morinaga, H. Itabashi, and S. Tanigawa, "Development of a permanent magnet motor utilizing amorphous wound cores," *IEEE Transactions on Magnetics*, vol. 46, no. 2, pp. 570–573, Feb 2010.

[6] N. Ertugrul, R. Hasegawa, W. L. Soong, J. Gayler, S. Kloeden, and S. Kahourzade, "A novel tapered rotating electrical machine topology utilizing cut amorphous magnetic material," *IEEE Transactions on Magnetics*, vol. 51, no. 7, pp. 1–6, July 2015.

[7] J. Ou, Y. Liu, M. Schiefer, and M. Doppelbauer, "A novel pm-free high-speed linear machine with amorphous primary core," *IEEE Transactions on Magnetics*, vol. 53, no. 11, pp. 1–8, Nov 2017.

[8] M. Alatalo, S. T. Lundmark, and E. A. Grunditz, "Electric machine design for traction applications considering recycling aspects-review and new solution," in *IECON 2011 - 37th Annual Conference of the IEEE Industrial Electronics Society*, Nov 2011, pp. 1836–1841.

[9] L. Hitachi Metals America, "Amorphous and Nanocrystalline-POWERLITE C-Cores," [Online]: https://www.hitachimetals.com/materials-products/amorphous-nanocrystalline/ powerlite-c-cores.php, October 2016, [Accessed]: Sept. 22, 2018.

[10] L. Advanced Technology & Materials Co., "Antaimo amorphous c-cores," [Online]: http://www.atmcn.com/Subsidiary/Metal/Products/3237.shtml, February 2018, [Accessed]: Sept. 22, 2018.

[11] J. F. Gieras, R. J. Wang, and M. J. Kamper, *Axial Flux Permanent Magnet Brushless Machines*. Dordrecht: Springer Netherlands, 2008.

[12] M. Aydin, S. Huang, and T. Lipo, "Axial flux permanent magnet disc machines: A review," *Conf. Record of SPEEDAM*, 01 2004.

[13] Y. Limited, "Yasa p400r series e-motor," [Online]: https://www.yasa.com/wp-content/uploads/2018/01/YASA_P400_Product_Sheet.pdf, 2018, [Accessed]: Mar. 01, 2019.

[14] A. Bettayeb, R. Kaczmarek, and J.-C. Vannier, "Analytical estimation of rotor loss due to stator slotting of synchronous pm machines," *World Academy of Science, Engineering and Technology*, vol. 66, 2010.

[15] Z. X. Fang, Z. Q. Zhu, L. J. Wu, and Z. P. Xia, "Simple and accurate analytical estimation of slotting effect on magnet loss in fractional-slot surface-mounted pm machines," in *2012 XXth International Conference on Electrical Machines*, Sep. 2012, pp. 464–470.

[16] A. G. Gonzalez, J. Millinger, and J. Soulard, "Magnet losses in inverter-fed two-pole pm machines," in *2016 XXII International Conference on Electrical Machines (ICEM)*, Sept 2016, pp. 1854–1860.

[17] A. G. Gonzalez, A. K. Jha, Z. Li, P. Upadhayay, and P. Rasmussen, "Validation of efficiency maps of an outer rotor surface mounted permanent magnet machine for evaluation of recyclability of magnets," in *2018 IEEE International Magnetic Conference (INTERMAG)*, April 2018, pp. 1–6.

[18] H. Domeki, Y. Ishihara, C. Kaido, Y. Kawase, S. Kitamura, T. Shimomura, N. Takahashi, T. Yamada, and K. Yamazaki, "Investigation of benchmark model for estimating iron loss in rotating machine," *IEEE Transactions on Magnetics*, vol. 40, no. 2, pp. 794–797, March 2004.